HHS Public Access

Author manuscript

Ann Biomed Eng. Author manuscript; available in PMC 2017 March 01.

Published in final edited form as:

Ann Biomed Eng. 2016 March ; 44(3): 816–827. doi:10.1007/s10439-015-1514-1.

Siloxane nanoprobes for labeling and dual modality imaging of neural stem cells

Caroline P. Addington, **Alex Cusick**, **Rohini Vidya Shankar**, **Shubhangi Agarwal**, **Sarah E. Stabenfeldt**[‡], and **Vikram D. Kodibagkar**[‡]

School of Biological and Health Systems Engineering, Arizona State University, Tempe, AZ 85287

Abstract

Cell therapy represents a promising therapeutic for a myriad of medical conditions, including cancer, traumatic brain injury, and cardiovascular disease among others. A thorough understanding of the efficacy and cellular dynamics of these therapies necessitates the ability to non-invasively track cells *in vivo*. Magnetic resonance imaging (MRI) provides a platform to track cells as a non-invasive modality with superior resolution and soft tissue contrast. We recently reported a new nanoprobe platform for cell labeling and imaging using fluorophore doped siloxane core nanoemulsions as dual modality (^{1}H MRI/Fluorescence), dual-functional (oximetry/detection) nanoprobes. Here, we successfully demonstrate the labeling, dual-modality imaging, and oximetry of neural progenitor/stem cells (NPSCs) *in vitro* using this platform. Labeling at a concentration of 10 μl/10^4 cells with a 40%v/v polydimethylsiloxane core nanoemulsion, doped with rhodamine, had minimal effect on viability, no effect on migration, proliferation and differentiation of NPSCs and allowed for unambiguous visualization of labeled NPSCs by ^{1}H MR and fluorescence and local pO_2 reporting by labeled NPSCs. This new approach for cell labeling with a positive contrast ^{1}H MR probe has the potential to improve mechanistic knowledge of current therapies, and guide the design of future cell therapies due to its clinical translatability.

Keywords

neural progenitor/stem cells; cell-labeling; polymethyldisiloxane; rhodamine; nanoemulsions; MR oximetry; fluorescence; dual-modality imaging

INTRODUCTION

Neural progenitor/stem cell (NPSC) transplants have shown promise in the context of neurodegenerative disease, stroke and traumatic injury within the central nervous system, making NPSC cell therapy an attractive candidate for translation to the clinic[11]. However, the mechanisms behind the benefits of NPSC therapies and their safety and efficacy remain unclear[11]. Evidence of this can be found in early clinical trials investigating fetal-derived neural stem cell grafts as a therapy for Parkinson's disease. While acute data indicated a

[‡]Corresponding Authors: 1) Sarah E. Stabenfeldt, School of Biological and Health Systems Engineering, Arizona State University, Tempe, AZ 85287, Sarah.Stabenfeldt@asu.edu. 2) Vikram D. Kodibagkar, School of Biological and Health Systems Engineering, Arizona State University, Tempe, AZ 85287, Vikram.Kodibagkar@asu.edu.

recovery of dopaminergic neuronal function[24], long-term success was highly variable. These trials were discontinued as many cases developed dyskinesia and two resulted in patient death[23]. As such, effective NPSC labeling for tracking transplants through clinically relevant, non-invasive imaging becomes necessary in looking towards a mechanistic understanding of cell-based therapies and their translation to the clinic. Effective methods to non-invasively track transplanted cells have the capacity to 1) understand the mechanism of existing therapies and 2) promote innovation and improvement of therapies currently in development.

Magnetic resonance imaging (MRI) is a widely used and extremely versatile clinical diagnostic tool because 1. it is non-invasive, 2. has no tissue depth penetration limitation at clinical fields and 3. provides both contrast among soft tissues at reasonably high spatial resolution and functional information related to tissue micro-architecture. The emergence of novel contrast agents (e.g. super-paramagnetic iron oxide or SPIO nanoparticles, micron-sized iron oxide particles or MPIOs and perfluorocarbon nanoparticles) has recently made possible *in vivo* real-time cell tracking with MRI[30]. The added benefit of superior soft tissue contrast of the underlying anatomy characteristic of MRI, allows for improvement in the accuracy of implant localization and visualization. However, the sensitivity of ^{1}H MRI is lower than other modalities particularly for cellular detection *in vivo* and is affected by several factors that are intrinsic to MRI such as the pulse sequence under consideration, coil geometry and sensitivity, optimal choice of scan parameters, and the field strength and homogeneity.

Many laboratories have investigated the feasibility of using conventional ^{1}H MRI to visualize immune cells, stem cells, and other cell types as reviewed recently[21,29,30]. Pioneering work with iron-oxide labeling visualized the presence and distribution of transplanted cells with negative contrast MRI (i.e. transplanted cells appear darker than background tissue)[8,13,16] as well as positive contrast (transplanted cells appear brighter than background tissue)[9,12]. Recent work also used ^{19}F based nanoprobes[3,5–7,28] to successfully label cells with a ^{19}F MRI contrast agent (perfluorocarbon (PFC) nanoemulsion) prior to transplantation, enabling simultaneous visualization of the disease pathology, tissue regeneration and transplanted cells via a dual ^{19}F/^{1}H approach with no background signal. Moreover, PFCs may also serve as an oxygen reporter thereby significantly expanding the capacity of MRI to report real-time molecular insight for cell therapy innovation[17]. However, wide use of ^{19}F MRI for routine human clinical application remains challenging, as most existing clinical scanners in hospitals cannot be easily modified to include ^{19}F MR capability. Even for dedicated research scanners, adding ^{19}F MR capability could involve expensive upgrades to hardware, software, and dual-tuned/wide-band tunable coils. As such, our efforts focused on developing a non-invasive cell tracking method that utilizes chemical-shift based positive signal contrast ^{1}H MRI to facilitate clinical translation.

We previously reported on Proton Imaging of Siloxanes to Map Tissue Oxygenation Levels (PISTOL), a technique that both tracks siloxanes and siloxane based nanoemulsions as MR positive contrast agents (via their unique chemical shift at 0 ppm) and also reports local pO_2 levels using ^{1}H MRI[15,18,20,24]. While our previous application of PISTOL focused on cancer diagnostic/prognostic technologies, the benefit of applying this reporter probe and the

associated imaging technique to cell transplant strategies is very self-evident. The nanoemulsion platform lends itself to incorporation of hydrophobic fluorescent dyes to enable dual MR and fluorescent imaging modalities[24] for *in vivo* imaging and *ex vivo* analysis. Therefore, this labeling paradigm has the potential to be a valuable tool from bench to clinic.

Neural progenitor/stem cell populations (NPSCs) are of specific interest to use as a benchmark transplant cell type as NPSC transplants have shown promise in neurodegenerative and traumatic brain injury models[11,27]. Magneto-dendrimers, SPIO and MPIO particles have been used in the past to label NPSCs with success[9,13,16]; however, iron oxide particle-labeled cells display a negative contrast signal much larger in volume than the implanted cell volume and are also susceptible to false positives in detection due to the characteristic MR signal voids of injured and neurodegenerative environments.

In this study, we investigated the behavior of NPSCs upon labeling with PDMS-core nanoemulsions loaded with a hydrophobic fluorophore and demonstrated dual-modality (^{1}H MR/fluorescence) imaging of labeled cells *in vitro*. In particular, we investigated the effect of labeling on NPSC proliferation, migration and differentiation, and all *in vitro* imaging studies were designed with future *in vivo* applicability in mind.

MATERIALS AND METHODS

Nanoparticle synthesis

Siloxane-based nanopropbes were synthesized as nanoemulsions based on our previously reported methods[15,24], with the use of polydimethylsiloxane (PDMS)/rhodamine B instead of hexamethylsiloxane (HMDSO)/Nile red as MR reporter/fluorophore, respectively. Briefly, nanoprobes were composed of PDMS/rhodamine B solution (40% v/v), deionized water (55% v/v) and Solutol® HS 15 (BASF Inc, Florham Park, NJ) as surfactant (5% v/v).

The PDMS/rhodamine B solution was prepared by dissolving a rhodamine-lipid conjugate (Lissamine Rhodamine B PE, Avanti Polar Lipids, Inc., Alabaster, AL) in chloroform (Sigma Aldrich, St. Louis, MO), subsequently heating to 40°C for 1 hr. PDMS (410 g/mol; Alfa Aesar, Ward Hill, MA) was then added and this solution was maintained under vacuum at 60 °C for 12 hrs to remove excess chloroform and yield a 0.25 mM rhodamine solution in PDMS. HS 15 was heated to a liquid state before mixing with deionized water (DIH_2O) in a 1:11 ratio at 70°C for 2 minutes. PDMS/rhodamine solution was then added drop-wise to the DIH_2O/HS 15 solution and allowed to sit at 70°C for 15 minutes prior to sonication for 45 minutes (3×15 minute intervals at 150W with a duty cycle of 50%) using a Omniruptor 4000 Ultrasonic Homogenizer (Omni International, Tulsa, OK). Nanoemulsions were filtered through 0.22 μm pore syringe filters 11 times prior to particle size measurement. The final concentration of Rhodamine B was 0.1 mM in the nanoemulsion. Nanoparticle diameter was characterized by Dynamic Light Scattering (DLS) (Delsa Nano Particle Size Analyzer, Beckman Coulter, Pasadena, CA), and mean diameter was obtained from 8 nanoemulsion samples.

NPSC isolation and culture

Neural progenitor/stem cells (NPSCs) were harvested from the medial and lateral germinal eminences of C57/BL6 E14.5 fetal mice according to protocols approved by the Arizona State University Institutional Animal Care and Use Committee. Briefly, mice were anesthetized at 3% isoflurane, rapidly decapitated, and fetuses were extracted from both uterine horns. Fetal tissue was rinsed in sterile, cold Leibovitz medium (Life Technologies, Carlsbad, CA) at each stage of the germinal eminence dissection. The germinal eminences were rinsed with sterile, cold Leibovitz medium before mechanical dissociation in working NPSC medium (glucose (6 ng/mL, Acros Organics, Geel, Belgium), HEPES buffer (5 mM, Sigma Aldrich, St. Louis, MO), progesterone (62.9 ng/mL, Sigma Aldrich), putrescine (9.6 μg/mL, Sigma Aldrich), heparin (1.83 μg/mL, Sigma Aldrich), B27 growth supplement (1X, Life Technologies), epidermal growth factor (20 ng/mL, Sigma Aldrich), fibroblast growth factor (5 ng/mL, Sigma Aldrich), insulin (5 μg/mL, Sigma Aldrich), transferrin (5 μg/mL, Sigma Aldrich), sodium selenite (5 ng/mL, Sigma Aldrich) in Dulbecco's Modified Eagle Medium (Life Technologies))and plated at a density of 10^4 cells/mL in a humidified incubator at 37°C, 20% O_2, and 5% CO_2. NPSCs were cultured as non-adherent neurospheres in working NPSC medium, passaged by mechanical dissociation, and utilized for experiments between passages 3 through 6.

NPSC Labeling and Viability

NPSC labeling was optimized with respect to viability by flow cytometry (BD Accuri C6, BD Biosciences, Franklin Lakes, NJ) where NPSCs in culture as neurospheres (3×10^5 cells per group) were supplemented with nanoparticle suspension at 1, 5, 10 or 50 μL/10^4 cells and incubated in humid conditions at 37°C for 1 hr. Following incubation, NPSCs were rinsed with fresh media prior to staining with calcein AM to label live NPSCs. For flow cytometry analysis of positive calcein AM, NPSCs were then spun down, rinsed with fresh media, and re-suspended at 10^5 cells/μL in sterile PBS + 0.1% bovine serum albumin (10^4 events counted per group). For fluorescence microscopy analysis, 100 μL NPSC suspension was pipetted onto a microscope slide and cover-slipped prior to imaging (DMI 6000B, Leica Microsystems, Wetzlar, Germany). Based on data presented in Figure 2 and Supplementary Figure 1, the 10 μL/10^4 cells labeling condition provided sufficient labeling with minimal impact on NPSC viability and was therefore used for subsequent experiments.

Effect of labeling on NPSC behavior

Proliferation—Labeled and unlabeled neurospheres were plated on poly-l-lysine (PLL) in 48-well plates (n=6, 10 μg/cm^2 PLL; MP Biomedicals, Solon, OH) at a density of 25 neurospheres/cm^2. After 6 days of culture in NPSC growth medium, NPSCs were digested in proteinase K solution for 72 hrs at 37°C and double-stranded DNA (dsDNA) was isolated with the Qiagen DNeasy kit (Qiagen, Venlo, Limburg, Netherlands). Quantification of dsDNA was performed by the Quant-iT PicoGreen dsDNA assay (Life Technologies) according to manufacturer's protocol and used as a measure of NPSC proliferation after normalizing to baseline measurements taken at the time of plating.

Migration—Labeled NPSCs and unlabeled NPSC controls were plated in ECM coated 24-well plates at 25 neurospheres/cm^2 (n=4 replicates per group; poly-L-lysine or laminin-1 (6 μg/cm^2; Sigma Aldrich), in mitogenic growth factor-free NPSC media. Cultures were imaged via phase contrast microscopy at 1, 3 and 6 days allowing for the tracking of radial NPSC migration out of the neurosphere. Images (n=6 per sample well) were analyzed for longest sphere diameter as shown in Figure 4 using a custom-designed MATLAB program (MathWorks, Inc., Natick, MA) and were normalized to baseline measurements taken 2 hours after plating.

Differentiation—Labeled and unlabeled neurospheres were cultured on laminin-1 coated glass coverslips as described previously in 24-well plates (n=4 replicates per group) for 6 days. NPSCs were then fixed with 3.7% paraformaldehyde (Sigma Aldrich), permeabilized with 0.1% Triton X 100 (Fisher Scientific, Houston, TX), and probed for proteins indicative of astrocytes (mouse anti-GFAP, Millipore, Billerica, MA), young neurons (mouse anti-β III Tubulin, Millipore), NPSCs (rabbit anti-nestin, Abcam, Cambridge, UK), and oligodendrocytes (rabbit anti-Olig2, Millipore). AlexaFluor488-conjugated goat anti-rabbit (Life Technologies) and AlexaFluor647-conjugated goat anti-mouse (Life Technologies) secondaries were used appropriately. DAPI (Life Technologies) was used for visualization of cell nuclei. Samples were imaged at 20X magnification via fluorescence microscopy (n=3 images per well; Leica, DMI4000 B).

Dual modality imaging of labeled NPSCs

All MR imaging was performed on a pre-clinical Bruker 7T scanner (Bruker, Billerica, MA) and the fluorescence imaging was performed using an IVIS-Spectrum instrument (PerkinElmer, Waltham, MA), both at the Barrow Neurological Institute-Arizona State University Center for Preclinical Imaging (Barrow Neurological Institute, Phoenix, AZ). Standard curves were generated based on known oxygenation levels (0, 10, and 21% O_2) at 23°C and 33.5 °C and used to calibrate PDMS nanoemulsion longitudinal relaxation rate, $R_1 = 1/T_1$, where T_1 is the longitudinal relaxation time, as a function of pO_2. NPSCs were labeled and 3 different imaging phantoms were prepared for dual modality MR/fluorescence imaging. The standard imaging protocol involved acquisition of T_1 and T_2 weighted scout scans to visualize the phantom, siloxane selective imaging using the PISTOL sequence [20] with proton density weighting to visualize the labeled NPSCs within the phantom. The MR imaging parameters employed were: FOV = 3×3 cm^2, TR/TE = 1000/25 ms, 64×64 matrix, slice thickness = 5 mm, in plane spatial resolution = 0.47×0.47 mm/pixel, scan time of 1s. Rhodamine selective fluorescence imaging ($\lambda_{ex}/\lambda_{em}$: 500 nm/560 nm) was performed to image the fluorophore label.

In the first phantom, a 750μL base layer of 2% agar was placed in the 2.0 mL microcentrifuge tube and placed on ice for cooling. Following gelation, 1.0 mL of labeled NPSC suspension (4×10^5 cells/mL, 1 hr labeling time) was added on top of the base layer and centrifuged at 1000 rpm for 5 minutes, forming a pellet on top of the agarose layer. A second 1.0 mL layer of liquid agarose was then gently pipetted on top of the cell pellet. This phantom was designed to simulate the scenario post-injection of a NPSC cell pellet *in vivo*.

A second imaging phantom was prepared using slightly different labeling parameters with an aim to increase labeling payload. Using 950,000 cells and a 3 hr incubation time, NPSCs were labeled. Instead of immersing the labeled pellet in two layers of agar, the NPSCs were washed in DPBS and re-suspended using 100 μL of agarose. This phantom was designed to replicate the injection of a NPSC loaded scaffold *in vivo*.

Finally a third phantom was made with the same procedure as phantom #1 (1 hr labeling time) with 10^5 cells (4 times less than phantom #1) to assess the sensitivity of the technique with our existing MR coils. This was then imaged using magnetic resonance spectroscopic imaging (MRSI, also referred to as chemical shift imaging or CSI) in addition to the standard imaging protocol described earlier. The MRSI acquisition parameters were: sequence= 2D point resolved spectroscopy (PRESS) based CSI, TR/TE = 1500/60 ms, FOV = 3×3 cm^2, 16×16×2048 matrix, spectral width = 4006 Hz, slice thickness = 4 mm, 1 average, in plane spatial resolution= 1.875×1.875 mm/pixel, spectral resolution = 0.98 Hz/pts, total scan time =6 min 24 s. A siloxane image was created from the MRSI data using MATLAB by integrating under the siloxane peak at every voxel, and overlaid on a scout image to display the location of NPSCs within the phantom. The ^1H resonance from PDMS is located at 0 ppm, (~1425 Hz up-field from water at 7T) on chemical shift spectra, similar to that of hexamethyldisiloxane[18]. Additionally, pO_2 was mapped with the PISTOL sequence by varying TR and number of averages as described in ref 20. The acquired T_1 weighted PISTOL images subsequently fit offline in MATLAB™ on a pixel-by-pixel basis using a custom built routine to generate the pO_2 map from the measured R_1 vs. pO_2 calibration curve (Supplementary Figure 3).

Statistical Analysis

All statistical analysis was performed in Prism 6 (GraphPad Software Inc., La Jolla, CA). NPSC proliferation data was analyzed by two-tailed t-test using Welch's correction for unequal standard deviations and α=0.05. NPSC migration data was analyzed by two-way ANOVA with Tukey's posthoc test and α=0.05. Flow cytometry analysis was performed in FlowJo (Tree Star Inc., Ashland, OR) where equivalent gating was performed for all samples.

RESULTS

Nanoemulsion labels NPSCs while maintaining viability

The nanoemulsion particle size was on an appropriate scale for cellular uptake, ranging from 50 – 150 nm and mean diameter of 98 ± 28 nm (Figure 1). Doping the nanoemulsions with the hydrophobic dye rhodamine B-PE facilitated fluorescent monitoring of cell labeling *in vitro* (Figure 2, Supplementary Figure 2). Flow cytometry data yielded a calcein AM-negative dead cell population (gating illustrated in Supplementary Figure 1), which increased as a function of labeling concentration. NPSC viability was maintained over 94% at 1 μL/10^4 cells, maintained over 80% at 5 and 10 μL/10^4 cells, then dropped to 64.60% at 50 μL/10^4 cells (Figure 2A). The two lowest labeling concentrations (1 and 5 μL/10^4 cells, Figure 2B, C) did not label NPSCs with detectable fluorescence intensity as observed with conventional fluorescence microscopy to enable distinction between labeled and unlabeled

NPSCs. Effective NPSC labeling was observed by fluorescence microscopy at the two higher concentrations (10 and 50 μL/10^4 cells, Figure 2D, E). Based on these data, 10 μL/10^4 cells labeling concentration provided the most effective labeling with minimal detriment to NPSC viability and, as such, was used for all subsequent experiments.

Labeling does not significantly affect NPSC proliferation

NPSC proliferation after 6 days in culture conditions was not significantly different between labeled and unlabeled populations ($p = 0.095$, Figure 3) as determined by PicoGreen dsDNA quantification. The unlabeled NPSC population was observed to increase by $1.12 \pm 0.21 \times 10^4$ cells where labeled NPSCs increased $1.31 \pm 0.21 \times 10^4$ cells compared to baseline measurements taken 2 hours after plating.

Labeling does not significantly affect NPSC migration

Labeled and unlabeled NPSC radial migration significantly increased on laminin compared to PLL at both days 3 and 6 ($p<0.001$ for both, Figure 4B, C). Moreover, there was no significant difference between labeled and unlabeled NPSC migration at 3 or 6 days on either PLL ($p=0.9979$, 0.9993, respectively) or laminin substrates ($p=0.9163$, 0.8901, respectively). It is important to note that the actively migrating cells from the central neurosphere at both days 3 and 6 remained labeled (Supplementary Figure 2), providing qualitative evidence that labeling does not negatively affect NPSC migration.

Labeling does not significantly affect NPSC differentiation

NPSC capacity for differentiation into young neurons, astrocytes and oligodendrocytes was not negatively affected by labeling after 6 days of culture on laminin (Figure 5). Labeled and unlabeled NPSCs stained positive at comparable levels for GFAP, a marker for astrocytes (Figure 5B, E), Olig2, a marker for young oligodendrocytes (Figure 5C, F) and beta III tubulin, a marker for young neurons (Figure 5H, K), after 6 days of culture on laminin in mitogenic growth factor-free culture media. A subset of the culture maintained nestin expression in both labeled and unlabeled NPSCs after 6 days of culture on laminin in mitogenic growth factor-free media indicating retention of neural progenitor phenotype (Figure 5I, L). Minimal Olig2 expression was observed for both labeled and unlabeled NPSCs under these culture conditions as expected based on previous work[1].

Labeled NPSCs can be detected by MR and fluorescence

Calibration curves obtained for the PDMS nanoemulsion displayed high pO_2 sensitivity with a linear dependence ($R^2>0.98$) of R_1 on pO_2 at 23 °C and 33.5 °C with slopes of $(1.30 \pm 0.08)\times10^{-3}$ (torr s)$^{-1}$ and $(1.25 \pm 0.01)\times10^{-3}$ (torr s)$^{-1}$ respectively (Supplementary Figure 3). The intercepts (representing the anoxic relaxation rate) were 0.235 ± 0.006 s^{-1} and 0.207 ± 0.001 s^{-1} at 23 °C and 33.5 °C respectively, which corresponds to a range of 4.3–4.8 s.

Figures 6 and 7 show the dual-modality imaging of the labeled NPSCs using a siloxane-selective MRI with the PISTOL sequence and fluorescence imaging. In the case of MR imaging of phantoms 1 and 2 (Figure 6), 10-fold lower signal-to-noise ratio (SNR) was observed for phantom 2 (SNR ~ 12.6, 64 signal averages, total imaging time = 3 min 12 s) when adjusted for the effect of number of signal averages, compared to phantom 1

(SNR~15.4, 1 signal average). Due to imaging time limitations, pO_2 measurements were not performed on these two phantoms. Using fluorescence imaging, a 7 fold lower signal-to-noise ratio (SNR) was obtained for phantom 2 (SNR~ 151) compared to phantom 1 (SNR~1000). In the case of phantom 3, siloxane selective imaging with PISTOL allowed detection and oximetry of cells with mean pO_2 value of 94±67 torr (Figure 7) for the pellet. MRSI also allowed the visualization of the labeled cells. The SNR for the proton density weighted PISTOL image (Figure 7B) was 12.3 while that of the MRSI chemical shift image (Figure 7E) was 38.6. In all cases fluorescence imaging easily showed the presence of labeled NPSCs and images from the two modalities were well correlated.

DISCUSSION

Cell-based therapies are a promising treatment strategy for a variety of clinical problems, ranging from degenerative diseases to cancer. However, the translation of cell-based therapies to the clinic has stalled largely due to questions related to efficacy and safety[11]. In moving from preclinical to clinical studies, the ability to critically analyze the fate and functional effects attributed to cell-based therapeutics is drastically limited due to the lack of non-invasive, nondestructive monitoring techniques. This major limitation has been identified by the California Institute of Regenerative Medicine and other agencies as a key obstacle in efforts to move stem cell therapies into the clinic[4]. Thus, the underlying mechanisms regarding the success or failures of such therapies in the clinic remain unclear. Development of effective cell labeling and non-invasive tracking methods would greatly facilitate the ability to monitor cell dynamics *in vivo* and evaluate the impact of cell therapies.

Improved detection of labeled cells could possibly be achieved using higher cell counts or increasing the amount label within a cell using longer incubation times or higher labeling concentration. However, this might have implications on cellular functionality. Our rhodamine doped PDMS-core nanoemulsion was found to effectively label NPSCs at a concentration of 10 μL/10^4 cells with robust fluorescent labeling retention out to 6 days (Supplementary Figure 1). These results are comparable to previous reports on superparamagnetic iron oxide (SPIO) particle labeling of NPSCs[16]. Labeling at 10 μL/10^4 cells maintained 80.1% NPSC viability (Figure 2), which is comparable to post-labeling viability in previous efforts to label NPSCs for non-invasive imaging with magnetic nanoparticles[26 and 19]F labeling agents[7]. We acknowledge that a post-labeling viability of 80% is less than optimal and thus continued experimentation with labeling parameters will be considered in future work to address this minor constraint.

Maintaining high viability is not, in itself, sufficient for effective cell labeling. NPSC behaviors such as proliferation, migration and differentiation are critical to the efficacy of NPSC transplant therapies, thus the effect of labeling techniques on these behaviors must be taken into account. Moreover, the mechanistic ambiguity surrounding cell therapy necessitates that the effects of labeling techniques on cellular behavior remain negligible. Labeling with PDMS nanoemulsion did not significantly affect NPSC proliferation, radial migration or capacity for differentiation into cell types of the CNS compared to unlabeled NSPCs (Figures 3–5) after 6 days in culture. While several published labeling techniques

have effectively conserved NPSC function, limited functionality of SPIO labeled cells *in vivo* has recently been reported by Cromer Berman et al[10]. Specifically, reduced migration of SPIO labeled NPSCs was observed compared to unlabeled NPSCs after transplantation *in vivo*, where early exocytosis of the particles appeared to allow for recovery of NPSC migration[10]. While PDMS labeled NPSC migration has not yet been investigated *in vivo*, the robust radial migration observed by labeled NPSCs *in vitro* without loss of labeling as observed for SPIO-labeled NPSCs indicates that PDMS labeling does not negatively affect NPSC migration and provides encouragement for forthcoming *in vivo* experimentation.

Dual-modality imaging and oximetry of labeled NPSCs was successfully demonstrated using ^{1}H MRI and fluorescence imaging for as low as 10^5 cells at 7T field (Figure 7). The individual SNR observed in each experiment indicate that further reduction of cell number would still allow detection within clinically acceptable imaging times (<10 min) but oximetry may be challenging. Surprisingly the SNR for the phantom with the least number of cells (phantom #3) was comparable to the other two phantoms with 4 times (phantom 1) and 9.5 times (phantom 2) as many cells. This implies that for future *in vitro* or *in vivo* studies, factors such as coil position relative to transplanted cells and coil tuning may be as critical for successful imaging and oximetry as efficient labeling. Furthermore, factoring in the acquisition time difference of 6.5 fold between the two sequences used for phantom 3, the PISTOL sequence would be theoretically expected to yield a SNR of 31.3 (compared to 38.6 for the MRSI sequence) for the same imaging time as the MRSI acquisition under these conditions. This indicates that the sensitivity of the PISTOL technique is only slightly lower than the MRSI. While the EPI based PISTOL has stricter limitation on minimum echo time, the SNR of the MRSI data could be improved by reduction in the echo time used. With the development of accelerated MRI data acquisition methods based on compressed sensing[23,34] and advanced radiofrequency coils for MRI[22,25,32], we can expect improved sensitivity of this and other positive contrast cell labeling techniques (such as using ^{19}F based probes[2]). Recently, Ahrens et al. have successfully imaged 10^7 perfluorocarbon emulsion-labeled dendritic cells in colorectal adenocarcinoma patients at 3T field with a custom-built surface coil[2], which is a promising development from the point-of-view of application of our analogous ^{1}H MR technique. It is important to note that recent developments using MPIOs for cell tracking[14] may enable detection and tracking of very small number of cells. While these particles cannot report on cellular pO_2, they show great potential for time-course migration studies with high resolution MRI if migration rates (not reported) remain unaltered with labeling.

Similar to perfluorocarbon based probes, oximetry of labeled cells by ^{1}H MR using siloxane-core nanoprobes requires mapping of the T_1 recovery time[19]. This currently takes 3.5 min using PISTOL assuming 1 signal average for the image acquired with the longest recovery time[20]. This long recovery time may pose a problem at low labeled-cell densities where signal to noise for a single shot acquisition may be <2.5 thus potentially hindering imaging and oximetry. For example, given that oximetry using PISTOL (with 1 average for the longest TR) takes 3.5 min, that for phantom 2 (with an SNR of 12.6 with 64 averages) would take 3 hrs and 44 min. In such cases, faster pulse-sequences will be needed to complete oximetry in clinically reasonable times. We recently reported[31] a faster version of

the PISTOL technique, that allows a temporal resolution of 1 min for oximetry using hexamethyldisiloxane (anoxic T_1~ 11 s). With PDMS, (anoxic T_1< 5 s) this new technique could perform single shot oximetry in 25s, thus allowing for signal averaging. In the present study, *in vitro* oximetry of labelled NPSC pellet (phantom 3) yielded a mean pO_2 value and range (94±67 torr) which is similar to that seen in case of MCF7 cells four hours after sealing the phantom[24]. While *in vivo* oximetry was not demonstrated in our study, we note that Zhong et al. successfully reported intracellular pO_2 measurements from labeled tumor cells *in vivo* and observed a transient spike in pO_2 following T-cell immunotherapy and putative tumor cell death[33]. Although, in this case, the target-cells were labeled as opposed to the therapeutic cells, this study highlights the importance of non-invasive, multifunctional tracking of cell therapy.

With any cell labeling technique, dilution of the intracellular label by cell division can potentially limit detection in the long-term. Internalization of the label nanoprobes by macrophages at the transplant site may obfuscate mechanistic interpretation of signal intensity time course from non-invasive imaging data. In this regard, the proposed technique has limitations equivalent to those of other positive or negative contrast cell-labeling techniques in development or clinical use[4].

In conclusion, we have successfully demonstrated *in vitro* labeling, imaging and oximetry of NPSCs using PDMS-based dual modality (MRI/fluorescence) nanoprobes with the potential for dual functionality (contrast/oximetry). Future work will aim to apply these nanoprobes to tracking implanted cells *in vivo* while simultaneously monitoring cell health via ^{1}H MR oximetry. The non-invasive nature of an MR based approach to cell tracking allows for increased applicability compared to destructive methods of cell tracking. As such, this tool has the potential to provide mechanistic insight into current therapies, allowing for informed innovation and improvement; and to guide the precise design of future cell therapies due to its clinical translatability.

Supplementary Material

Refer to Web version on PubMed Central for supplementary material.

Acknowledgments

The authors would like to acknowledge David Menn, Arizona State University, and Qingwei Liu, Barrow Neurological Institute, for technical assistance. These studies were supported by a Rising Stars in Engineering seed grant from College of Engineering, ASU (VDK and SES) and NIH 1DP2HD084067 (SES).

References

1. Addington CP, Pauken CM, Caplan MR, Stabenfeldt SE. The role of SDF-1α-ECM crosstalk in determining neural stem cell fate. Biomaterials. 2014; 35:3263–3272. [PubMed: 24438907]
2. Ahrens ET, Zhong J. In vivo MRI cell tracking using perfluorocarbon probes and fluorine-19 detection. NMR Biomed. 2013; 26:860–871. [PubMed: 23606473]
3. Ahrens ET, Flores R, Xu H, Morel PA. In vivo imaging platform for tracking immunotherapeutic cells. Nat Biotech. 2005; 23:983–987.
4. Bhirde A, Xie J, Swierczewska M, Chen X. Nanoparticles for cell labeling. Nanoscale. 2011; 3:142–153. [PubMed: 20938522]

5. Bible E, Dell'Acqua F, Solanky B, Balducci A, Crapo PM, Badylak SF, Ahrens ET, Modo M. Non-invasive imaging of transplanted human neural stem cells and ECM scaffold remodeling in the stroke-damaged rat brain by 19F- and diffusion-MRI. Biomaterials. 2012; 33:2858–2871. [PubMed: 22244696]
6. Boehm-Sturm P, Mengler L, Wecker S, Hoehn M, Kallur T. In Vivo Tracking of Human Neural Stem Cells with 19F Magnetic Resonance Imaging. PLoS ONE. 2011; 6:e29040–9. [PubMed: 22216163]
7. Bonetto F, Srinivas M, Heerschap A, Mailliard R, Ahrens ET, Figdor CG, de Vries IJM. A novel 19F agent for detection and quantification of human dendritic cells using magnetic resonance imaging. Int J Cancer. 2010; 129:365–373. [PubMed: 20839261]
8. Bulte JWM, Zhang SC, van Gelderen P, Herynek V, Jordan EK, Duncan ID, Frank JA. Neurotransplantation of magnetically labeled oligodendrocyte progenitors: Magnetic resonance tracking of cell migration and myelination. Proceedings of the National Academy of Sciences. 1999; 96:15256–15261.
9. Bulte J, Bulte JW, Douglas T, Douglas T, Witwer B, Witwer B, Zhang SC, Strable E, Strable E, Lewis BK, Lewis BK, Zywicke H, Zywicke H, Miller B, Miller B, van Gelderen P, Moskowitz BM, Moskowitz BM, Duncan ID, Frank JA. Magnetodendrimers allow endosomal magnetic labeling and in vivo tracking of stem cells. Nat Biotech. 2001; 19:1141–1147.
10. Cromer Berman SM, Kshitiz CJ, Wang I, Orukari A, Levchenko JWM, Bulte, Walczak P. Cell motility of neural stem cells is reduced after SPIO-labeling, which is mitigated after exocytosis. Magn Reson Med. 2012; 69:255–262. [PubMed: 22374813]
11. De Feo D, Merlini A, Laterza C, Martino G. Neural stem cell transplantation in central nervous system disorders. Current Opinion in Neurology. 2012; 25:322–333. [PubMed: 22547103]
12. Gilad AA, Walczak P, McMahon MT, Na HB, Lee JH, An K, Hyeon T, van Zijl PCM, Bulte JWM. MR tracking of transplanted cells with "positive contrast" using manganese oxide nanoparticles. Magn Reson Med. 2008; 60:1–7. [PubMed: 18581402]
13. Granot D, Scheinost D, Markakis EA, Papademetris X, Shapiro EM. Serial monitoring of endogenous neuroblast migration by cellular MRI. NeuroImage. 2011; 57:817–824. [PubMed: 21571076]
14. Granot D, Nkansah MK, Bennewitz MF, Tang KS, Markakis EA, Shapiro EM. Clinically viable magnetic poly(lactide-co-glycolide) particles for MRI-based cell tracking. Magn Reson Med. 2014; 71:1238–1250. [PubMed: 23568825]
15. Gulaka PK, Rastogi U, McKay MA, Wang X, Mason RP, Kodibagkar VD. Hexamethyldisiloxane-based nanoprobes for 1H MRI oximetry. NMR Biomed. 2011; 24:1226–1234. [PubMed: 21412864]
16. Guzman R, Uchida N, Bliss TM, He D, Christopherson KK, Stellwagen D, Capela A, Greve J, Malenka RC, Moseley ME, Palmer TD, Steinberg GK. Long-term monitoring of transplanted human neural stem cells in developmental and pathological contexts with MRI. Proceedings of the National Academy of Sciences. 2007; 104:10211–10216.
17. Janjic JM, Ahrens ET. Fluorine-containing nanoemulsions for MRI cell tracking. WIREs Nanomed Nanobiotechnol. 2009; 1:492–501.
18. Kodibagkar VD, Cui W, Merritt ME, Mason RP. Novel1H NMR approach to quantitative tissue oximetry using hexamethyldisiloxane. Magn Reson Med. 2006; 55:743–748. [PubMed: 16506157]
19. Kodibagkar VD, Wang X, Mason RP. Physical principles of quantitative nuclear magnetic resonance oximetry. Frontiers in bioscience: a journal and virtual library. 2008; 13:1371–1384. [PubMed: 17981636]
20. Kodibagkar VD, Wang X, Pacheco-Torres J, Gulaka P, Mason RP. Proton imaging of siloxanes to map tissue oxygenation levels (PISTOL): a tool for quantitative tissue oximetry. NMR Biomed. 2008; 21:899–907. [PubMed: 18574806]
21. Kraitchman DL, Bulte JWM. In vivo imaging of stem cells and Beta cells using direct cell labeling and reporter gene methods. Arteriosclerosis, Thrombosis, and Vascular Biology. 2009; 29:1025–1030.
22. Laistler E, Poirier-Quinot M, Lambert SA, Dubuisson RM, Girard OM, Moser E, Darrasse L, Ginefri JC. In vivo MR imaging of the human skin at subnanoliter resolution using a

superconducting surface coil at 1.5 tesla. J Magn Reson Imaging. 2013; 41:496–504. [PubMed: 24382749]

23. Lustig M, Donoho D, Pauly JM. Sparse MRI: The application of compressed sensing for rapid MR imaging. Magn Reson Med. 2007; 58:1182–1195. [PubMed: 17969013]
24. Menon JU, Gulaka PK, McKay MA, Geethanath S, Liu L, Kodibagkar VD. Dual-Modality, Dual-Functional Nanoprobes for Cellular and Molecular Imaging. Theranostics. 2013; 2:1199–1207. [PubMed: 23382776]
25. Nabuurs RJA, Hegeman I, Natté R, van Duinen SG, van Buchem MA, van der Weerd L, Webb AG. High-field MRI of single histological slices using an inductively coupled, self-resonant microcoil: application to ex vivo samples of patients with Alzheimer's disease. NMR Biomed. 2011; 24:351–357. [PubMed: 20960578]
26. Ramos-Gómez M, Seiz EG, Martínez-Serrano A. Optimization of the magnetic labeling of human neural stem cells and MRI visualization in the hemiparkinsonian rat brain. J Nanobiotechnology. 2015; 13:20. [PubMed: 25890124]
27. Riess P, Zhang C, Saatman KE, Laurer HL, Longhi LG, Raghupathi R, Lenzlinger PM, Lifshitz J, Boockvar J, Neugebauer E. Transplanted neural stem cells survive, differentiate, and improve neurological motor function after experimental traumatic brain injury. Neurosurgery. 2002; 51:1043–1054. [PubMed: 12234415]
28. Ruiz-Cabello J, Walczak P, Kedziorek DA, Chacko VP, Schmieder AH, Wickline SA, Lanza GM, Bulte JWM. In vivo "hot spot" MR imaging of neural stem cells using fluorinated nanoparticles. Magn Reson Med. 2008; 60:1506–1511. [PubMed: 19025893]
29. Srinivas M, Aarntzen EHJG, Bulte JWM, Oyen WJ, Heerschap A, de Vries IJM, Figdor CG. Imaging of cellular therapies. Advanced Drug Delivery Reviews. 2010; 62:1080–1093. [PubMed: 20800081]
30. Srivastava AK, Kadayakkara DK, Bar-Shir A, Gilad AA, McMahon MT, Bulte JWM. Advances in using MRI probes and sensors for in vivo cell tracking as applied to regenerative medicine. Disease Models & Mechanisms. 2015; 8:323–336. [PubMed: 26035841]
31. Vidya Shankar, R.; Kodibagkar, VD. A rapid Look-Locker imaging sequence for quantitative tissue oximetry. Proc. SPIE 9417, Medical Imaging 2015: Biomedical Applications in Molecular, Structural, and Functional Imaging; 2015. p. 94170F
32. Wang ZJ. Improving SNR of RF coils using composite coil elements. NMR Biomed. 2009; 22:952–959. [PubMed: 19582771]
33. Zhong J, Sakaki M, Okada H, Ahrens ET. In Vivo Intracellular Oxygen Dynamics in Murine Brain Glioma and Immunotherapeutic Response of Cytotoxic T Cells Observed by Fluorine-19 Magnetic Resonance Imaging. PLoS ONE. 2013; 8:e59479–7. [PubMed: 23667419]
34. Zhong J, Mills PH, Hitchens TK, Ahrens ET. Accelerated fluorine-19 MRI cell tracking using compressed sensing. Magn Reson Med. 2012; 69:1683–1690. [PubMed: 22837054]

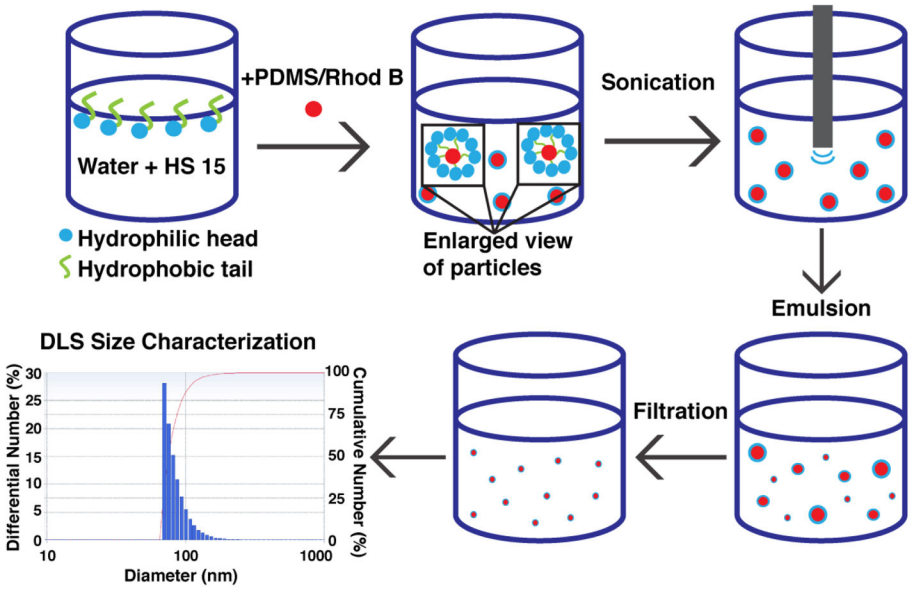

Figure 1.

Nanoprobe fabrication process of PDMS/Rhodamine B-loaded emulsions. HS 15 emulsifier encapsulates PDMS/Rhodamine B in aqueous solution. Nanoemulsions are formed through sonication and then filtered to exclude larger particles. Dynamic light scattering (DLS) data indicate that particles range from 50–150 nm in diameter after filtration, number-weighted average is 98 ± 28 nm (average of 8 samples).

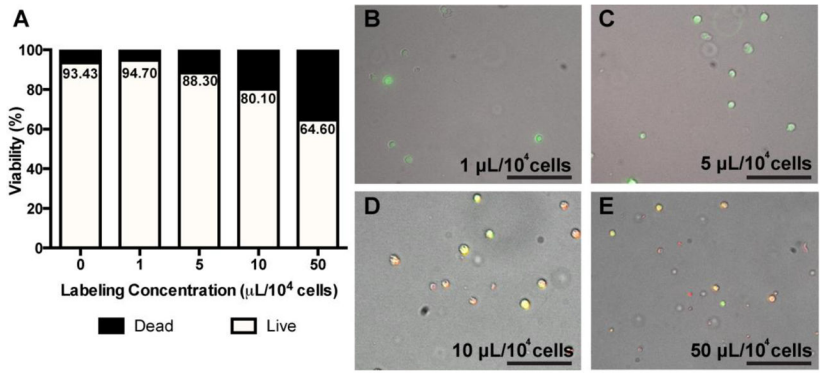

Figure 2.

NPSC viability after nanoemulsion labeling. Percent viability decreased as a function of labeling concentration, observed as a calcein AM negative NPSC population through flow cytometry (A). Effective labeling, determined through fluorescent microscopy, was not observed at 1 or 5 μL/10^4 cells compared to unlabeled NPSCs (AC) but was detectable in NPSCs labeled at 10 and 50 μL/10^4 cells (D, E). Fluorescent imaging of calcein AM positive NPSCs supports flow cytometry data where viability is well preserved up to 50 μL/10^4 cells, at which point it decreases substantially. Scale bars are 50 μm.

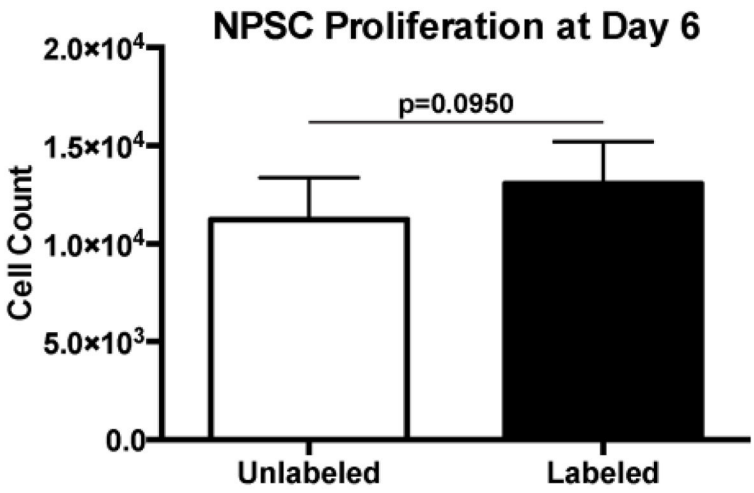

Figure 3.

NPSC proliferation on poly-L-lysine (PLL) at 6 days as determined through PicoGreen dsDNA quantification. Cell counts were not significantly different after 6 days of culture on PLL between labeled and unlabeled NPSCs (p=0.0950). Cell counts were calculated based on a cell standard and normalized to baseline measurements at taken day 0.

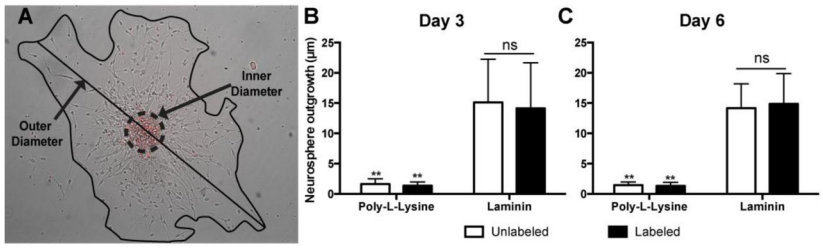

Figure 4.

NPSC radial migration on poly-L-lysine (PLL) and laminin out to 6 days. NPSC radial migration was quantified through diametrical measurements at days 3 and 6 normalized to baseline measurements taken at day 0(A). Both labeled and unlabeled NPSC radial migration significantly increased on laminin at days 3(B) and 6(C) compared to labeled and unlabeled PLL controls, respectively. No significant differences were observed between radial migration of unlabeled and labeled NPSCs on laminin at 3 (B) and 6 (C) days. *$p<0.01$ compared to unlabeled NPSC migration on laminin, #$p<0.01$ compared to labeled NPSC migration on laminin.

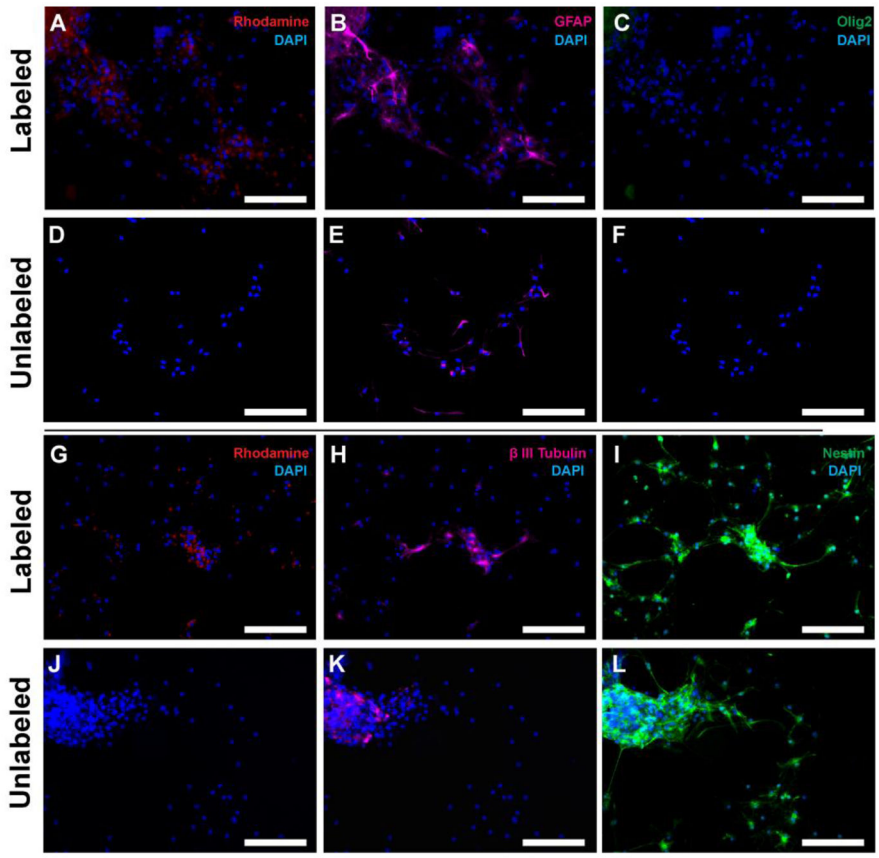

Figure 5.

NPSCs retain capacity for differentiation out to 6 days after labeling as compared to unlabeled NPSCs. Labeled cells, indicated by positive rhodamine signal (A, G), stained positive for markers of astrocytes (GFAP,B), young oligodendrocytes (Olig2,C) and young neurons (β III tubulin, H) in levels comparable to those of unlabeled NPSCs (D–F, J–L). A subset of labeled and unlabled cells retained NPSC phenotypic markers as indicated by positive nestin staining (I, L, respectively). Scale bar is 150 μm.

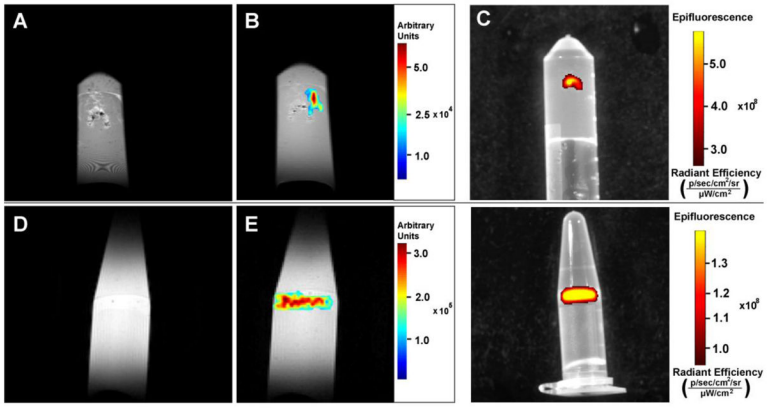

Figure 6.

Dual-modality (MRI/fluorescence) imaging of labeled NPSC pellet (phantom 1, 4×10^5 cells) (A-C) and labeled NPSCs (phantom 2, 9.5×10^5 cells) suspended in agarose (D–F). T_1-weighted scout scan of labeled stem cell pellet submerged in agarose gel (A, D), siloxane-selective proton density PISTOL image overlaid on scout image (B, E), and fluorescence ($\lambda_{ex}/\lambda_{em}$ = 500 nm/560 nm) image (C, F).

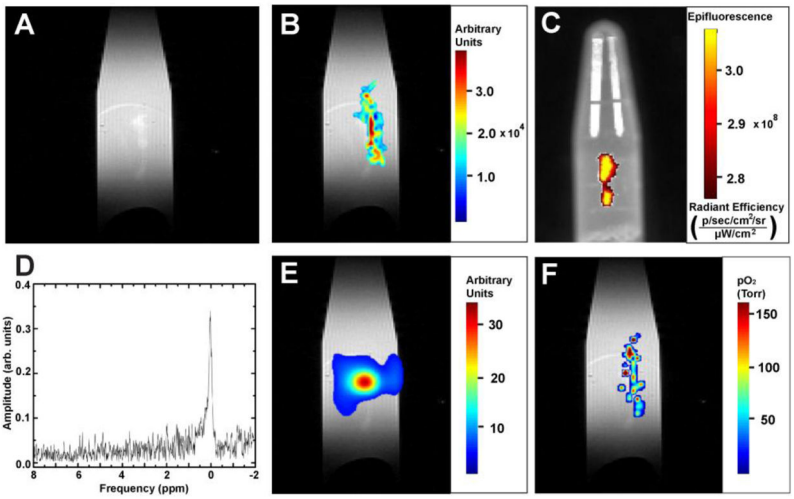

Figure 7.

Dual-modality (MRI/fluorescence) imaging and oximetry of labeled NPSC pellet (1×10^5 cells) in phantom 3. (A) T_1-weighted scout image (B) siloxane-selective proton density PISTOL image overlaid on scout image (C) fluorescence ($\lambda_{ex}/\lambda_{em}$ = 500 nm/560 nm) image, (D) water-suppressed NMR spectra of high intensity voxel in the metabolite map, (E) chemical shift image (0 ppm) overlaid on scout image, and (F) pO_2 map overlaid on scout image.